Quasi-one-dimensional ultracold rigid-rotor collisions: Reactive and nonreactive cases

R. Vexiau
Laboratoire Aimé Cotton, CNRS, Université Paris Sud, ENS Cachan, Université Paris Saclay, 91405 Orsay Cedex, France

J.-M. Launay and A. Simoni
Univ Rennes, CNRS, IPR (Institut de Physique de Rennes)-UMR 6251, F-35000 Rennes, France

(Received 21 January 2019; revised manuscript received 6 June 2019; published 8 July 2019)

We study polar alkali-metal dimer scattering in a quasi-one-dimensional geometry for both reactive and nonreactive species. Elastic and reactive rates are computed as a function of the amplitude of a static electric field within a purely long-range model with suitable boundary conditions at shorter range. We describe the diatomic molecules as rigid rotors and results are compared to the fixed-dipole approximation. We show in particular that for molecules with a sufficiently strong induced dipole moment oriented perpendicular to the trap axis, the long-range repulsive interaction leads to the suppression of short-range processes. Such shielding effect occurs for both reactive and nonreactive molecules, preventing two-body reactions as well as losses due to complex-mediated processes [M. Mayle *et al.*, Phys. Rev. A **85**, 062712 (2012)] from occurring. The present results demonstrate the possibility to suppress loss rates in current ultracold molecule experiments using one-dimensional confinement.

DOI: 10.1103/PhysRevA.100.012704

I. INTRODUCTION

Ultracold molecules have added a new twist to the field of cold atoms [1,2]. The first groundbreaking experiments were carried out several years ago at JILA, where a dense gas of ultracold fermionic KRb dimers was produced by two-photon association [3]. This molecular species is reactive, a feature that has been explored in the context of quantum-state controlled chemical reactions [4]. However, from the standpoint of many-body studies, the reactivity of KRb is, in general, a drawback leading to fast particle loss from the trap.

More recently, different groups have reported the production of *nonreactive* ultracold alkali-metal dimers [5–10]. Such molecules, if prepared in the absolute single-particle energy state, are strictly stable under two-body collisions. However, there is experimental evidence that even under these favorable conditions, inelastic losses still occur at a fast pace [6–8,10]. This is true in particular for bosonic molecules, whereas fermionic samples appear to be more stable [9]. A mechanism that might explain the observed losses is related to the existence of Fano-Feshbach resonances available with high density at thermal energies even in an ultracold gas. The presence of such resonances increases the collision lifetime of a pair of molecules, creating a tetrameric complex. Such metastable complex can be lost from the trap since it is not necessarily trapped in the optical lattice and can undergo recombination to deeper levels by colliding with a third molecule, a process often referred to as "sticky collision" [11,12]. Excitation of the complex by the trapping laser has also been recently proposed as an alternative mechanism that might explain the observed loss rates [13].

In order to increase the sample lifetime, it is therefore important to devise strategies to prevent molecules from approaching at short distances, where detrimental inelastic processes take place. Unfortunately, in three dimensions, there always exists an attractive head-to-tail reaction path leading to the short range. This circumstance has been shown to result in a strong dependence $\sim d^6$ of the reactive rate on the induced dipole moment d [14]. More subtle quantum effects have been proposed to control the reaction dynamics of alkali-metal dimers prepared in rotationally excited states [15]. Microwave shielding leading to a dramatic lifetime increase has also been recently theoretically studied [16,17].

The situation is different if molecules are confined in tight traps, for instance by optical means. In fact, confinement can then be easily designed in such a way that molecule pairs will tend to collide in a *repulsive* side-to-side configuration, the head-to-tail pathway being energetically unfavored by the confining potential. This approach has been demonstrated both experimentally and theoretically to lead to a drastic increase of the lifetime of reactive polar molecules trapped in one and two spatial dimensions [18–21].

Our previous study of reactive collisions in one-dimensional optical tubes has addressed highly reactive species [21]. Therein, polar molecules have been simply described as fixed dipoles of magnitude equal to the induced dipole moment. Resonances have been found to be strongly quenched by inelastic processes and have no influence on the scattering cross sections. The aim of the present work is twofold. First, we relax the fixed-dipole approximation by explicitly introducing the rotational degrees of freedom of the colliding diatoms. Second, in addition to studying reactive collisions, we introduce a model for nonreactive molecules, in which scattering cross sections can indeed be dominated by dense resonance spectra. We compare both reactive and nonreactive rigid-rotor models with the fixed-dipole approximation. As a main result, we show that resonances in elastic

cross sections and thus possibly complex-mediated collisions can be suppressed using the dipole-dipole repulsion induced by an applied electric field.

The paper is organized as follows. Section II introduces the formalism and our numerical approach. Section III presents the long-range multipolar expansion of the molecule-molecule interaction. Results for different dialkali-metal species and collision energies are presented as a function of an applied electric field in Sec. IV. A short conclusion summarizes this work.

II. FORMALISM

We consider two molecules A and B confined in a quasi-one-dimensional geometry by a potential approximated as a harmonic trap. The quadratic nature of the confining potential allows one to separate center-of-mass and relative motion. The rigid-rotor Hamiltonian describing the collision in relative coordinates includes the kinetic energy, the confinement potential, and an interaction term V_{int} defined below in Eq. (2), which includes intermolecular forces and the Stark interaction energy with the external electric field. In this work, we will describe the dimer molecules as rigid rotors, an approximation valid as long as the intermolecular distance remains large compared to the extent of the internal coordinates.

The kinetic energy of the dimer + dimer complex will be decomposed into a sum of three independent terms depending, respectively, on the relative distance $\mathbf{R}$ between the two centers of mass, the internal coordinate of the dimer A, and the internal coordinate of dimer B [22]. Furthermore, we will assume that the dimers remain in their vibrational ground level, reducing the dimer contribution to the kinetic energy to a purely rotational term.

Putting all terms together, the total Hamiltonian reads

$$\begin{aligned} H &= T_R + T_{\text{rot}} + V_{\text{trap}} + V_{\text{int}} \\ &= -\frac{\hbar^2}{2\mu}\frac{d^2}{dR^2} + \frac{\boldsymbol{\ell}^2}{2\mu R^2} + \frac{1}{2}\mu\omega_\perp^2\rho^2 + B_v\mathbf{J}_A^2 + B_v\mathbf{J}_B^2 \\ &\quad + V_{\text{int}}(\mathbf{R}). \end{aligned} \tag{1}$$

Here, $\boldsymbol{\ell}$ is the orbital angular momentum of the relative motion, $\mathbf{J}_A$ and $\mathbf{J}_B$ are the angular momenta of A and B with rotational constant B_v, $\omega_\perp = 2\pi\nu_\perp$ is the trap frequency, and ρ is the distance to the trap axis z. We use, for each molecule, the spectroscopically determined rotational constant B_v of the ground level $X^1\Sigma^+; v = 0$. The values and reference of the spectroscopic study can be found in [23]. The transverse oscillator length characterizing the trap size will be defined as $a_{\text{ho}} = \sqrt{\hbar/(\mu\omega_\perp)}$. As demonstrated in three spatial dimensions, hyperfine interactions would greatly increase the complexity of the problem [11,12]. However, we do not expect such added complexity to bring novel qualitative features to the main effects that we wish to demonstrate and hyperfine interactions will be neglected in this work.

We will now extend to rigid rotors the computational approach developed for fixed dipoles in our previous work [21]. Our method to construct the scattering wave function consists in a simultaneous expansion of the angular part of the solution in a suitable internal basis whereas the radial coordinate is discretized on a grid of points. The radial discretization is detailed in Sec. II A. The angular basis comprises the orbital angular coordinate $\hat{R}$ as well as any internal degree of freedom of the diatomic, as described in Sec. II B.

A. Radial discretization

The radial discretization is performed according to the spectral element approach [24,25]. Briefly, we choose a minimum r_c and a maximum r_{max} radial distance and define a solution interval $I = [r_c, r_{\text{max}}]$, which is in turn partitioned into a set of N nonoverlapping sectors. A number of grid points and a basis set of Gauss-Lobatto cardinal functions associated with those points are assigned to each sector. The wave function is represented on the discrete basis and continuity of the wave function and of its radial derivative is enforced at the connection points between sectors. This strategy results in a highly sparse matrix in the grid indices. It should be remarked that our method allows different angular bases to be used in each sector. With the basis over all coordinates defined, we can rewrite the Schrödinger equation as a linear system that can be solved for a matrix solution Ψ in the interval I provided boundary conditions are assigned at the endpoints r_c and r_{max}.

At the right endpoint, we impose $\Psi'(r_{\text{max}}) = \mathbf{I}$; the matrix solution at r_{max} then becomes equal to the R matrix defined as $\mathbf{R} \equiv \Psi(\Psi')^{-1}$. From $\mathbf{R}$, one can then extract the scattering matrix and hence all physical observables such as the elastic and reactive collision rates [18,21].

We will impose two different boundary conditions at r_c. The first assumes that at short distance, the molecules react with unit probability. We thus require that the spherical surface $R = r_c$ is totally absorbing, i.e., across the surface we only have incoming flux and no reflected outgoing flux. In practice, we first define local adiabatic channels $|\alpha\rangle$ and corresponding energies E_α by diagonalizing the angular Hamiltonian $T_{\text{rot}} + V_{\text{int}}$ at distance $R = r_c$. Next, we assume that the wave function can be described by a pure incoming spherical wave in each channel α for $R \simeq r_c$. The logarithmic derivative $Z(r_c) \equiv \Psi'(r_c)\Psi^{-1}(r_c)$ is therefore diagonal with elements $(-ik_\alpha - \frac{1}{2}k'_\alpha k_\alpha^{-1/2})$, where $k_\alpha = \sqrt{2\mu(E_{\text{coll}} - E_\alpha)/\hbar^2}$ is the channel wave vector and the derivative is taken with respect to R. This method has been shown to give accurate prediction for dialkali-metal reactive species [26].

Our second approach amounts to the Dirichlet boundary condition $\Psi = \mathbf{0}$, i.e., the wave function is required to have a nodal surface for $R = r_c$. In this description, we can observe resonances between the incoming open channel with collision energy E_{coll} and bound levels of closed channels with energy close to E_{coll}. Since the radius r_c is chosen arbitrarily and there is *a priori* no reason for the wave function to have a nodal surface for $R = r_c$, we cannot predict the location of the resonances in terms of the amplitude of the electric field. As a matter of fact, the short-range collision parameters (more precisely, the quantum defects; see [11,12]) can be considered as stochastic variables arising from the extremely complex four-body dynamics taking place inside r_c. In this view, our specific Dirichlet condition can be considered as one possible realization of such complex process.

The specific value $r_c = 40\,a_0$ has been chosen so to satisfy the following criteria. First, the rigid-rotor model is expected to be accurate in the external region $R > r_c$. Second, motion

is semiclassical near r_c for the adsorbing model of Ref. [26] to apply. Finally, since we are interested in resonance spectra, the density of states near the threshold must be the same for the Dirichlet "truncated potential" as for the full one. We have checked that for our choice of r_c, this holds true up to energies of the order of 1 K in the case of a single deep potential well with van der Waals tail.

The present approach can therefore be expected to give useful insight into the collisions dynamics and it allows us to compare, on an equal footing, different approaches, namely, the fixed-dipole and the rigid-rotor descriptions. Finally, note that for the sake of comparison, we will use the nonreactive Dirichlet condition even for intrinsically reactive species such as LiCs or LiRb.

B. Angular basis

The angular part of the wave function in the rigid-rotor model is expanded in the so-called decoupled basis $|J_A M_A, J_B M_B, l M_l\rangle$ representation defined by the operators $\mathbf{J}_A^2$, $\mathbf{J}_B^2$, $\boldsymbol{\ell}^2$ with eigenvalues $\hbar^2 J_A(J_A+1)$, $\hbar^2 J_B(J_B+1)$, and $\hbar^2 l(l+1)$, as well as by their projections on the laboratory axis with eigenvalues M_A, M_B, and M_l. The laboratory axis is taken as the axis of the confining optical tube. In parallel configuration, where the electric-field axis is aligned along the laboratory axis, the projection of the total angular momentum, $M \equiv M_A + M_B + M_l$, is conserved, allowing us to work with a smaller basis set. For nonparallel configurations, one has to take into account couplings between different M due to the electric field.

The interaction potential matrix included in Eq. (1),

$$\mathbf{V}_{\rm int}(R) = \frac{\mathbf{C}_3}{R^3} + \frac{\mathbf{C}_6}{R^6} + \mathbf{V}_{{\rm Stark},A} + \mathbf{V}_{{\rm Stark},B}, \tag{2}$$

comprises the dipole-dipole interaction $\mathbf{C}_3/R^3$, the van der Waals interaction $\mathbf{C}_6/R^6$, and the Stark term arising from the interaction between the molecular dipoles $\mathbf{d}_{A,B}$ and the electric field. The matrix elements of $\mathbf{C}_3$ and $\mathbf{C}_6$ depend on the angular momenta J_A, J_B, and l as well as their projection on the laboratory axis. They are obtained using the Wigner-Eckart theorem, and their expression in the space-fixed frame can be found in [27–30]. For completeness, here we report the expression of the dipole-dipole interaction,

$$\begin{aligned}\langle J_A' M_A J_B' M_B' l' M_l' | \frac{\mathbf{C}_3}{R^3} | J_A M_A J_B M_B l M_l\rangle = -\sqrt{30}\frac{d^2}{R^3}\sum_{m_1 m_2}(-1)^{M_A'+M_B'+M_l'}\sqrt{[J_A][J_A'][J_B][J_B'][l][l']}\begin{pmatrix}1 & 1 & 2\\ m_1 & m_2 & -m_1-m_2\end{pmatrix}\\ \times\begin{pmatrix}J_A' & 1 & J_A\\ 0 & 0 & 0\end{pmatrix}\begin{pmatrix}J_A' & 1 & J_A\\ -M_A' & m_1 & M_A\end{pmatrix}\\ \times\begin{pmatrix}J_B' & 1 & J_B\\ 0 & 0 & 0\end{pmatrix}\begin{pmatrix}J_B' & 1 & J_B\\ -M_B' & m_2 & M_B\end{pmatrix}\begin{pmatrix}l' & 2 & l\\ 0 & 0 & 0\end{pmatrix}\begin{pmatrix}l' & 2 & l\\ -M_l' & -m_1-m_2 & M_l\end{pmatrix},\end{aligned} \tag{3}$$

where the common abbreviation $[X] = 2X+1$ has been used. The Stark term represents an internal interaction that acts on the degrees of freedom of the individual molecule. The term for molecule A (B) is therefore diagonal in the quantum numbers of molecule B (A) as well as in the orbital quantum numbers $l M_l$. The matrix elements are given explicitly for the molecule of label A by

$$\langle J_A' M_A' | \mathbf{V}_{{\rm Stark},A} | J_A M_A\rangle = -\mathcal{E}\langle J_A' M_A' | d_{z,A} | J_A M_A\rangle = \mathcal{E} d\sqrt{[l][l']}\begin{pmatrix}J_A' & 1 & J_A\\ 0 & 0 & 0\end{pmatrix}\begin{pmatrix}J_A' & 1 & J_A\\ -M_A' & 0 & M_A\end{pmatrix} \tag{4}$$

in terms of the electric-field intensity $\mathcal{E}$, a formally identical equation holding for B. The electronic van der Waals interaction is, in general, anisotropic [31]. However, we have explicitly taken into account the anisotropic contribution for the study of KRb + KRb and found it to give negligible corrections to the computed scattering observables. Therefore, only the isotropic contribution will be included in our model.

A few additional points must be taken into consideration. First, since we focus on collisions of identical diatomics, we need to use symmetrized wave functions,

$$\left|\Psi_{J_A M_A J_B M_B l M_l}\right\rangle = \frac{\left|J_A M_A J_B M_B l M_l\right\rangle + (-1)^l |J_B M_B J_A M_A l M_l\rangle}{\sqrt{2\left(1+\delta_{J_A J_B}\delta_{M_A M_B}\right)}}. \tag{5}$$

For the perpendicular electric-field configuration, the Hamiltonian is also symmetric with respect to reflection across the plane orthogonal to the trap axis and containing the origin. We can construct a symmetrized wave function,

$$\left|\Psi^{\epsilon}_{J_A M_A J_B M_B l M_l}\right\rangle = \frac{\left|\Psi_{J_A M_A J_B M_B l M_l}\right\rangle + (-1)^{\epsilon+M_A+M_B+M_l}\left|\Psi_{J_A -M_A J_B -M_B l -M_l}\right\rangle}{\sqrt{2\left(1+\delta_{M_A 0}\delta_{M_B 0}\delta_{M_l 0}\right)}}. \tag{6}$$

Last, while the decoupled basis is useful in the weak electric-field regime, for higher amplitudes, different J levels are heavily mixed by the field, and the system is better described in a dressed basis set [32,33]. To obtain this basis, we numerically diagonalize, for each field amplitude, the diatomic potential $B_v \mathbf{J}_X^2 + V_{{\rm Stark},X}$ $(X = A, B)$. We thus get the eigenfunctions

$|\widetilde{J}\widetilde{M}_J\rangle = \sum_J \alpha_J |JM_J\rangle$, which are in turn combined into the tetrameric wave function $|\widetilde{J}_A\widetilde{M}_A\widetilde{J}_B\widetilde{M}_B l M_l\rangle$. In order to compute the total potential matrix, we first evaluate the matrix elements in the decoupled basis and then we numerically evaluate

$$\langle \widetilde{J}'_A\widetilde{J}'_B l'|H|\widetilde{J}_A\widetilde{J}_B l\rangle = \sum_{J_A J_B J'_A J'_B} \alpha_{J_A}\alpha_{J_B}\alpha_{J'_A}\alpha_{J'_B}\langle J'_A J'_B l'|H|J_A J_B l\rangle, \tag{7}$$

where the magnetic quantum numbers have been suppressed for notational convenience.

The rigid-rotor description is only used between $R = 40\,a_0$, chosen as the r_c boundary value in this work, and $R = 200\,a_0$. For intermediate distances above $R = 200\,a_0$, the dipole-dipole interaction between different rotational level is weak compared to the energy gap of those level. One can thus focus on the rotational ground level with $\widetilde{J}_A = 0$ and $\widetilde{J}_B = 0$, using perturbation theory to take into account excited levels; see Sec. III. Spherical harmonics $|lM_l\rangle$ are still used to represent orbital motion.

Finally, in the long-range domain, typically $R > 10^4\,a_0$, the cylindrical confining potential of the two-dimensional trap overcomes the molecule-molecule interaction, limiting $\hat{R}$ to a small angular region around the pole. A development in spherical harmonics becomes increasingly inefficient and we use cylindrical grid basis functions projected on the spherical surface that stay localized near the pole as R varies. As an order of magnitude, a few-hundred spherical harmonics are needed to enforce continuity at the connection point between the intermediate and the long-range regions.

We will compare the rates obtained with the current approach to results from our previous model where fixed dipoles were used instead of rigid rotors [21]. In the latter, the interaction between the molecule in its rotational ground level and the Stark field is described as a point particle with a given induced permanent dipole moment. All rotational effects factor into a unique C_6 long-range coefficient. The total angular wave function is expanded on a basis of orbital spherical harmonics and the Hamiltonian only contains the orbital kinetic energy, the confinement potential, and the interaction potential V_{int}. Such point-particle model is equivalent to our intermediate-range rigid-rotor model, where we include only the rotational ground state, though the correction to the C_6 coefficient needs to be taken the same in both models; see Sec. III.

III. INDUCED DIPOLE MOMENT INTERACTION

Some care must be taken in the definition of the C_6 matrix coefficient in order to have a correct description of the van der Waals interaction. Two different approaches are used in this work.

In the first one, used for the intermediate-range domain or for the point-particle model, excited rotational states are not explicitly included in the basis. Resulting from a second-order perturbation treatment, the C_6 coefficient is thus written as a sum over all excited rotational, vibrational, and electronic levels of both molecules. Following Refs. [23,34], the C_6 can be decomposed into the sum of two contributions, i.e., a term C_6^e including the electronic transitions contribution and one C_6^r including the rotational transition contribution. Pure vibrational transitions as well as cross terms have been shown to be negligible [23]. Values of the C_6^e are taken from [23]. The C_6^r term is described in more detail in Sec. III A.

In the second approach, used for the short-range domain, the rotational states are explicitly included in the basis. The second-order term is thus coming only from the electronic transitions C_6^e. An additional corrective term is, however, needed to prevent the appearance of unphysical levels; see Sec. III B.

As mentioned above, in both cases, the C_6^e is taken as a purely isotropic term.

A. Rotational transition contribution

Due to the competition between the electric field and the rotational Hamiltonian, the rotational spectrum is heavily perturbed. A field-free C_6^r value would thus not be appropriate [35].

In more detail, the expression of the rotational contribution is

$$C_6^r = \sum_{(\widetilde{J}_A,\widetilde{J}_B)\neq(\widetilde{0},\widetilde{0})} \frac{|\langle \widetilde{J}_A, \widetilde{J}_B|\mathbf{d}_A\cdot\mathbf{d}_B|\widetilde{0},\widetilde{0}\rangle|^2}{\Delta E_A + \Delta E_B}, \tag{8}$$

with ΔE_A (ΔE_B) being the energy difference between the ground and the excited J_A (J_B) level. Dependence on the space-fixed projections M_A and M_B of the excited rotational levels is omitted in the formula for ease of reading. For the field-free case, $\widetilde{J} \equiv J$, and the only nonzero transition is from $J = 0$ to $J = 1$. We then obtain the expression for two identical molecules,

$$C_6^r(\mathcal{E} = 0) = \frac{d_{\text{perm}}^4}{4B_v}, \tag{9}$$

with d_{perm} the permanent dipole moment of the diatomic, expressed in its own molecular frame.

To obtain more accurate results for the collision rate, we compute an improved C_6^r value using Eq. (8) at each electric-field amplitude. We note that for a nonzero field, the heteronuclear molecules present an induced permanent dipole moment in the laboratory frame. In this case, the contribution of matrix elements such as $\langle\widetilde{0},\widetilde{1}|\mathbf{d}_A\cdot\mathbf{d}_B|\widetilde{0},\widetilde{0}\rangle$ is non-negligible. Those transition terms with one molecule in the ground level and the other in an excited one are related to the induction interaction C_6^{ind}, while the remaining transitions involving two rotationally excited molecules added to the electronic C_6^e form the dispersion coefficient C_6^{disp}.

Rotational contributions have been shown to be small for heteronuclear molecules LiNa and KRb due to their weak permanent dipole moment [23]. However, for a molecule such as LiCs, they are by far the dominant term. In Fig. 1, we show the difference in C_6 coefficients for LiCs-LiCs interactions depending on the model used. Calculations were performed with a single C_6^e term, a fixed field-free C_6 term, a field-dependent C_6^{disp} term, and, finally, a field-dependent $C_6^{\text{disp}} + C_6^{\text{ind}}$ term. At weak fields, the difference between the values obtained at the different levels of approximation is small and the collision rate is essentially the same for each model. At higher fields, the dominant term is the C_3 dipole-dipole interaction and

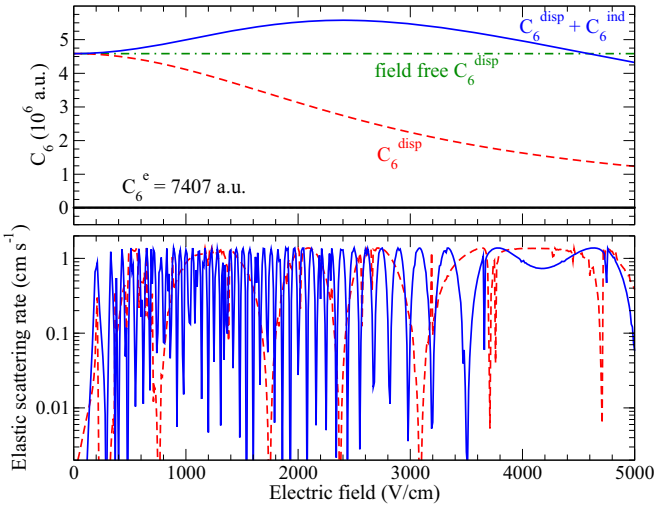

FIG. 1. Upper panel : van der Waals C_6 coefficient for LiCs-LiCs interaction. The electric field is parallel to the trap axis. Four different models were used: an electronic C_6^e (full line at 7407 a.u.) added to a rotational field-free C_6^r term (dashed line) or a field-dependent C_6^r (dot-dashed line) added to the induction coefficient $C_6^{\rm ind}$ (solid line). Lower panel : elastic collision rate at $E_{\rm coll} = 50$ nK imposing the Dirichlet boundary condition at short range computed for van der Waals coefficient C_6^r (solid line) or $C_6^r + C_6^{\rm ind}$ (dashed line).

modifications of the C_6 coefficient have no major impact on our results. However, the C_6 interaction is still relevant at short intermolecular distances.

The bottom panel in Fig. 1 shows the elastic collision rate computed using model potentials built with and without the induction interaction. Calculations are performed at low collision energy with the Dirichlet boundary condition at short range, such that scattering is purely elastic. The calculated collision rate presents several resonant features associated to the presence of quasibound states. The origin of these features will be discussed in more detail in Sec. IV. It is, however, important to remark here, as apparent from the figure, that their density at large electric fields is severely underestimated if one omits the induction interaction.

B. Unphysical states

When neglecting the rotation in the point-particle model, we still need to compute a corrective C_6 term, which means that the modification of the rotational structure must be taken into account in the model in second-order perturbation theory. In a similar fashion, the use of the rigid-rotor basis mentioned in Sec. II B leads to unphysical states if no correction is made [36,37]. Indeed, due to computational limitations, one has to truncate the basis, neglecting all the levels with $\widetilde{J} > \widetilde{J}_{\rm max}$. In particular, all of the coupling matrix elements of the type $\langle \widetilde{J}_A' \widetilde{J}_B' l' | V | \widetilde{J}_A \widetilde{J}_B l \rangle$ with either J_A' or J_B' above the angular momenta $\widetilde{J}_{\rm max}$ are cut off. Rotational levels with $J = \widetilde{J}_{\rm max}$ are the most affected by this truncation [36,37]. To reduce the effect of this approximation on the ground state, and thus on the collision rate, one can simply increase the size of the basis.

Another approach is to use second-order perturbation theory. In this approximation, the omitted couplings are assumed to be a perturbation to the levels included in our basis, giving rise to a corrective term $V_{\rm corr}$ to be added to the Hamiltonian. This term is diagonal with matrix elements

$$\langle \widetilde{J}_A \widetilde{J}_B l | V_{\rm corr} | \widetilde{J}_A \widetilde{J}_B l \rangle = \sum_{\widetilde{J}_A' \widetilde{J}_B' > \widetilde{J}} \frac{|\langle \widetilde{J}_A' \widetilde{J}_B' l | V | \widetilde{J}_A \widetilde{J}_B l \rangle|^2}{\Delta E_A + \Delta E_B}, \qquad (10)$$

where the sum is over every level above the cutoff angular momentum and V is the dominant coupling term, i.e., the dipole-dipole interaction C_3/R^3 in our case. The square of the matrix element on the right-hand side leads to a R^{-6} correction to the C_6 coefficient. In this work, we take $\widetilde{J}_{\rm max}$ equal to either 1 or 2, and the sum is carried out up to $\widetilde{J} = 7$. The energy gap ΔE is taken as the diatomic energy gap, thus neglecting the molecule-molecule interaction.

IV. RESULTS

We perform calculations for different bosonic species under various trapping conditions, collision energy, and electric field. Table I resumes the relevant characteristic physical parameters relevant for our calculations. The van der Waals length $\bar{a} = (2\mu C_6/\hbar^2)^{1/4}/2$ given in the table represents the average scattering length for collisions in a pure C_6/R^6 potential and can be interpreted as the range of such potential [38]. Here we focus on an intermediate confinement regime, which we define following Ref. [39] as $a_{\rm ho} \approx 10\,\bar{a}$. The collision energy of the identical heteronuclear molecules will be fixed in most calculations to 50 nK. With reference to the table, one can remark that for a heavy molecule such as LiCs, such collision energy can be considered as "hot" in terms of the trap level spacing. In fact, the gap with the first-excited energy level of the transverse harmonic oscillator is only slightly larger than twice the collision energy.

We first consider the configuration where the electric field is parallel to the confinement axis. In this case, molecules tend to be in attractive head-to-tail configuration and to react at the cutoff radius r_c.

This intuitive picture is confirmed by the analysis of the adiabatic potentials, obtained by diagonalizing the total interaction potential at each value of the interparticle distance R. Note that at parallel configuration, the projection of the orbital angular momentum on the trap axis is conserved and it has been fixed to $M_l = 0$. One can observe in Fig. 2 that the lowest adiabatic curve, the one that to first approximation controls the dynamics, presents no potential barrier preventing the molecules from reaching the short-range reactive region. On the converse, the more excited adiabatic potentials present, at short range $\sim 50 a_0$, a barrier arising from the centrifugal potential. The rotational degrees of freedom correspond to the excited thresholds ~GHz in the leftmost panel of Fig. 2. Each rotational manifold presents, in turn, a finer energy structure due to the transverse harmonic trap levels with equal spacing $h\nu_\perp$; see rightmost panel of Fig. 2.

Coming to the dynamics, we find that for the universal reactive model, the effect of the rotationally closed channel is minor. In fact, as shown in the upper panel of Fig. 3, the elastic collision rates computed within the rigid-rotor and the fixed-dipole models are essentially identified. The difference is more pronounced when taking the Dirichlet boundary

TABLE I. Relevant numerical parameters used in our calculation, as defined in the text. The reference collision energy E_{coll} is 50 nK. Two confinement strengths, intermediate and strong, are indicated for the LiRb dimer. Numbers in square brackets indicate the power of 10.

	$\bar{a}$ (units of a_0)	a_{ho} (units of a_0)	$\nu_\perp$ (kHz)	$E_{\text{coll}}/\hbar\omega_{\text{perp}}$	d_{perm} (a.u.)	B_v (GHz) [23]
^{39}K ^{87}Rb	117	955	10	1.6[-2]	0.242	1.13
^{7}Li ^{39}K	224	2236	5	3.3[-2]	1.410	7.69
^{7}Li ^{87}Rb	325	2473	2	8.3[-2]	1.645	6.46
Strong		341	100	1.6[-3]		
^{7}Li ^{133}Cs	497	6408	0.2	8.3[-1]	2.201	5.62
^{23}Na ^{87}Rb	355	2286	2	8.3[-2]	1.304	2.09

condition, as illustrated in the lower panel. When the scattering phase crosses a multiple of π, a broad zero crossing is observed in both the rigid-rotor and the fixed-dipole calculations. This happens near 2500 V/cm in both models, with a relative shift of a few-hundred V/cm. A second zero occurs near 5000 V/cm. By analogy with the Ramsauer-Townsend effect, which occurs as a function of collision energy, in the following we will briefly refer to such zeros as Ramsauer minima.

Most importantly, for rigid-rotor collisions, we observe resonance effects, manifesting themselves as a series of narrow features superimposed to the slowly varying background. As in the case of atoms, such resonances can, in principle, be used to control the dimer-dimer scattering properties through an applied field. In this work, we do not attempt a precise resonance assignment, which would require, for instance, quasi-bound-state or reduced adiabatic calculations. However, the fact that such resonances are absent in the fixed-dipole calculation strongly suggests that the ones in the figure are of rotational origin, i.e., they can be assigned to some potential curve correlating with rotationally excited molecules. A related study of true (as opposed to quasi-)bound states of molecules in a quasi-1D geometry can be found in [40].

We now focus on a system where the electric field is perpendicular to the trap axis. It can be expected that in this configuration and with a strong enough induced permanent dipole moment, the diatomic molecules will repel each other at long range [39] and can be protected against short-range reactive collisions. Figure 4 shows the elastic and reactive collision rates for LiK molecules calculated with the fully absorbing boundary condition. Results obtained in the fixed-dipole approximation are virtually indistinguishable from the rigid-rotor model and are not shown. In particular, the reactive rate is suppressed by about three orders of magnitude in the considered range of $\mathcal{E}$, confirming that the shielding phenomenon is robust versus rotation. Also note from the figure that the elastic rate presents a much more pronounced minimum in the elastic cross section as compared to KRb. This happens since, due to the small magnitude of the reactive rate for large electric field, LiK collisions are essentially elastic and the minimum is not quenched by inelastic processes as happens for KRb.

Not all molecules have indeed sufficiently strong dipole moment and thus dipole-dipole repulsion to suppress reactive processes. In general, molecules with a large intrinsic dipole moment and a small rotational constant are more polarizable,

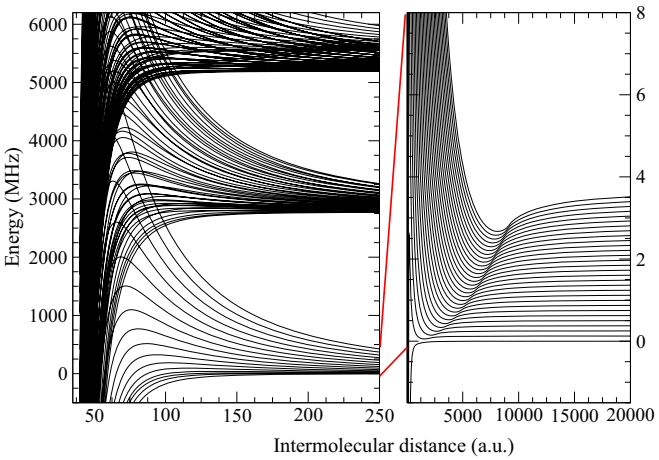

FIG. 2. Adiabatic potential curves for a KRb + KRb system in the presence of a static electric field of 5 kV/cm parallel to the trap axis. Left panel: the short-range intermolecular-distance domain; right panel: the intermediate-range distance domain. Transition from a dipolar-dominated system to a 1D confined system is indicated by the "ridge" visible at intermediate distances in the right panel. Electric field of 5 kV/cm is parallel to the trap axis.

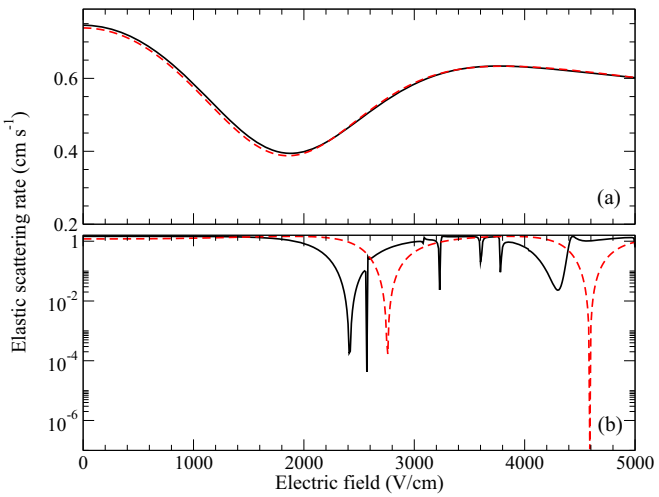

FIG. 3. Elastic collisions rate between two KRb molecules, described as rigid rotor (solid line) or fixed dipole (dashed line), in a quasi-1D geometry as a function of the amplitude of the electric field, oriented parallel to the trap axis. (a) Rates computed with a unitary loss at short range. (b) Rates computed using the Dirichlet boundary condition.

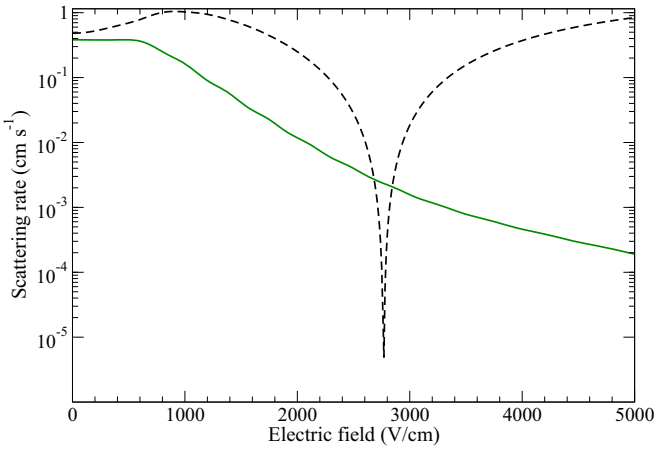

FIG. 4. Reactive (solid line) and elastic (dashed line) collisions rate between two LiRb molecules in a quasi-1D geometry as a function of the amplitude of the electric field, oriented perpendicular to the trap axis. Results are for a rigid-rotor model, indistinguishable on the figure scale from the ones for fixed dipoles (not shown).

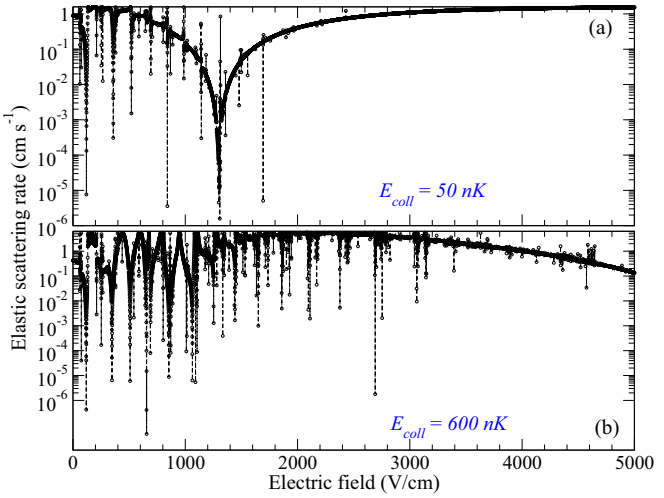

FIG. 6. Elastic collision rate for NaRb + NaRb collisions as a function of the amplitude of the electric field, perpendicular to the trap axis. Collision energy is (a) 50 and (b) 600 nK. The Dirichlet boundary condition is imposed at short range.

the induced electric dipole in the laboratory frame is larger, and thus the shielding is more effective in these systems for a given electric field. To confirm this trend, we have carried out sample calculations with the trapping parameters from Table I corresponding to intermediate confinement and found that the only molecules not having a strong enough permanent dipole moment to obtain significant shielding effects are LiNa and KRb.

We now consider nonreactive species, taking the NaRb dimer as an example. The long-range adiabatic curves of the NaRb-NaRb tetrameric taken for different amplitudes of the static electric field are shown in Fig. 5. Each adiabatic potential correlates asymptotically with an energy level $h\nu_\perp(n+1)$ of the isotropic transverse harmonic oscillator with principal quantum number n and degeneracy $(n+1)$. At shorter distance, the dipolar interaction becomes significant and breaks the isotropy of the oscillator. The dipolar interaction contributes, for instance, an energy of d^2/R^3 for molecules oscillating in the plane perpendicular to the dipoles and $d^2/R^3[1-3\cos^2(\theta)]$ for molecules in the plane containing the dipoles and the trap axis, with θ the angle between **R** and **d**. This anisotropy leads to the lifting of the asymptotic degeneracy clearly visible in the three panels of the figure as the intermolecular distance decreases.

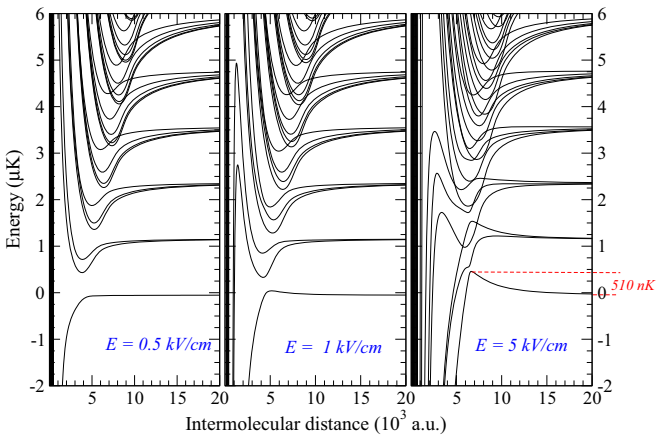

FIG. 5. Adiabatic potential curves for a NaRb + NaRb system. Left panel: with a weak static electric field of 0.5 kV/cm; middle panel: with a field of 1 kV/cm; and right panel: with a strong field of 5 kV/cm.

Moreover, as expected at perpendicular configuration, a barrier to reaction is formed in the lowest adiabatic potential as the amplitude of the field increases. To experience a significant short-range dynamics, the molecules would need to tunnel through this barrier, which, for instance, at 5 kV/cm has height of 510 nK; see rightmost panel of Fig. 5. Under this field-induced shield, it is interesting to compare the dynamics of a collision with a collision energy well below the maximum of the barrier (50 nK), and slightly over the top of the adiabatic potential barrier (600 nK).

Figure 6 shows the results of calculations performed with the Dirichlet boundary condition. With reference to Fig. 6(a), one may once again remark a Ramsauer minimum near 1200 kV/cm at the lowest considered collision energy. The minimum shifts at larger electric fields, outside the range of Fig. 6(b), at larger collision energy. In fact, quite generally, a potential has less influence on faster particles and, in order to have the accumulated phase shift go through π, larger values of $\mathcal{E}$ are needed. The main scattering feature is the dense spectrum of overlapping resonances observed at both considered collision energies. Such resonances arise from the coupling between the incoming channel and the closed channels, either correlating with the trap or with rotationally excited level.

The resonances observed in both panels of Fig. 6 have positions essentially independent of collision energy, as expected since a collision energy of the order of nK is essentially negligible on the scale of the Stark shift, $-d\mathcal{E}$. Note, however, that both the line shape and the resonance widths vary

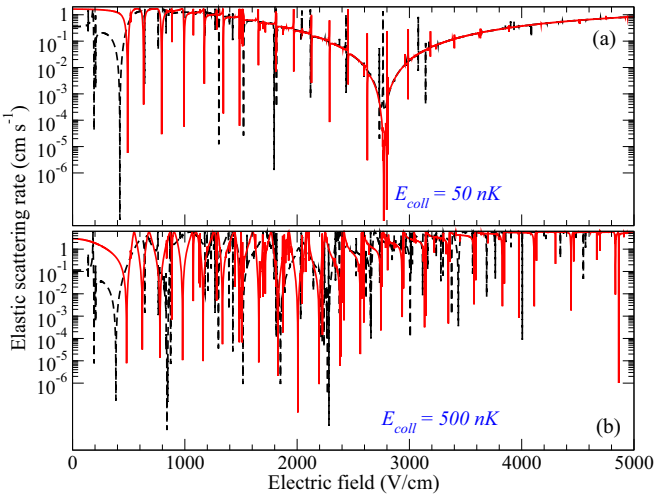

FIG. 7. Same as Fig. 6, but for LiRb + LiRb collisions. Solid red lines correspond to the rigid-rotor model; black dashed lines correspond to the fixed-dipole one. Collision energy is (a) 50 and (b) 500 nK. Plot is for transverse confinement $\nu_\perp = 2$ kHz and Dirichlet boundary condition.

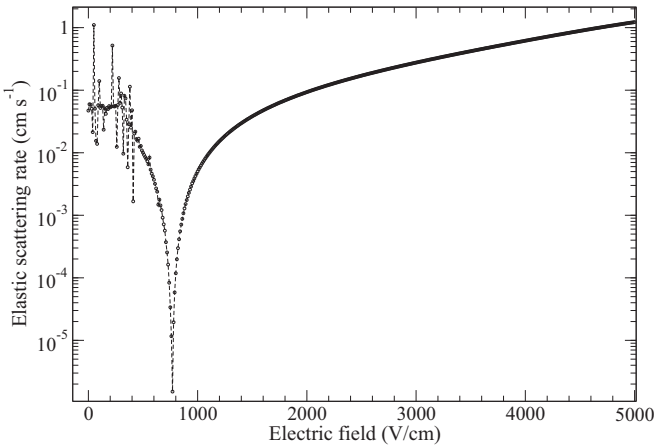

FIG. 8. Elastic collision rate for LiRb + LiRb collisions as a function of the electric-field amplitude for the rigid-rotor model. Plot is for tight transverse confinement with $\nu_\perp = 100$ kHz and Dirichlet boundary condition.

significantly between the two panels of Fig. 6. Most importantly, at low collision energy [Fig. 6(b)], resonance effects tend to be washed out in particular at strong fields, say above $\mathcal{E} \sim 2000$ kV/cm, since the adiabatic barrier becomes increasingly high and broad. In other terms, the presence of the barrier tends to keep the molecules far apart and prevents resonance effects, which are due to a *short-range* coupling between the open and the closed collision channels, from occurring. At larger collision energy barrier tunneling is more effective and resonances only begin to disappear near the upper limit of the figure, $\mathcal{E} \sim 5000$ kV/cm.

As conjectured in [11,12], resonant population of dense quasibound states increases the collision lifetime along with the probability of loss of the untrapped complex and of inelastic recombination via collision with a third body. These phenomena are suspected to be a significant limiting mechanism to the lifetime of ultracold quantum gases [6–8]. According to the present results, resonances can be suppressed in 1D geometries. Confinement combined with a strong static electric field and low temperatures should thus allow one to shield nonreactive molecules from complex-mediated collisions in addition to shielding reactive molecules.

In order to confirm such conclusion on a different molecular species, we consider a nonreactive LiRb model; see Fig. 7. As for NaRb, at the smaller collision energy of Fig. 7(a), the resonance width strongly decreases with $\mathcal{E}$, resonances first tend to become nonoverlapping, and their influence on the background cross section finally vanishes. The presence of a Ramsauer minimum, its shift, and the behavior of the resonance width with increasing collision energy [Fig. 7(b)] follow the same trend observed in NaRb.

Figure 7 also shows an interesting comparison with the fixed-dipole approximation. Note that as expected, the density of resonant features is larger for the rigid-rotor model due to the additional rotational degrees of freedom of the dimers. However, the density of resonances observed in the fixed-dipole model, thus purely due to trap confinement and tuned via the Stark energy shift, is significant in this system. Shielding becomes otherwise effective at comparable values of the electric field at each considered collision energy. It is worthwhile to compare Fig. 7(a) with Fig. 4, both referring to the same molecular system and physical parameters, but with different (nonreactive vs reactive) boundary conditions. Such comparison makes clear the fact that the scattering rate for the *reactive* LiRb model in Fig. 4 presents virtually no structure, not due to the absence of electrically tuned quasibound states, but rather because resonance effects are strongly quenched by fast reactive decay.

Let us finally consider the effect of confinement. On physical grounds, for dipoles perpendicular to the axis, stronger transverse confinement should further help preventing particles from approaching. In fact, dipoles in side-by-side configuration repel and can only get close by moving away from the trap axis towards an attractive head-to-tail configuration. In terms of adiabatic potentials, this means that the barrier in the lowest adiabatic curve will be stronger at a given electric field for a more confining than for a looser harmonic trap.

This picture is confirmed by Fig. 8, which shows the elastic collision rate for a nonreactive LiRb + LiRb collision model in a strong confinement regime. The resonance spectrum appears relatively sparse even at relatively low electric fields, meaning again that coupling between the open channel and quasibound states is weak since particles are prevented from reaching the short-range coupling region. This result extends to nonreactive systems the conclusion of Ref. [39], which demonstrated within the fixed-dipole approximation a more marked suppression of reactive processes occurring in tight traps. As expected, inclusion of rotation does not seem to change this general conclusion that basically depends on the presence of a potential barrier formed at long range, in a region where the fixed-dipole approximation is an excellent one.

Overall, it seems possible to find conditions for stabilizing the gas against inelastic processes of both reactive and complex-mediated nature to the extent that a suitable balance

between low temperatures, confinement, and electric-field intensity is found.

V. CONCLUSIONS

We have presented a rigid-rotor model to study identical polar molecule collisions in a quasi-1D optical trap. Collisions of reactive molecules in the rotational ground state are well described in the fixed-dipole approximation. The present calculation confirms that for sufficiently strong induced dipole moments, electrostatic repulsion between dipoles perpendicular to the trap axis leads to suppression of the reactive rates. For nonreactive molecules, the rotational degrees of freedom result in an increased density of Fano-Feshbach resonances. We demonstrate that the resonance widths decrease and resonance spectra dramatically decongest for increasing induced electric dipole moment of the molecules. This effect could be exploited to decrease the collision lifetime and possibly to suppress harmful processes due to the formation of an intermediate long-lived complex.

In perspective, it can also be interesting to model experiments where collision dynamics has been studied in the presence of an additional optical lattice along the axis of the tube [20]. This computational task could be accomplished, for instance, by combining the present 3D solution strategy and the asymptotic reference Bloch functions constructed in [41]. The effect of hyperfine interactions could also be included in the model to various levels of approximation.

ACKNOWLEDGMENTS

This work is supported by the Agence Nationale de la Recherche (Contract COLORI No. ANR-12-BS04-0020-01).

[1] L. D. Carr, D. DeMille, R. V. Krems, and J. Ye, New J. Phys. **11**, 055049 (2009).
[2] G. Quéméner and P. S. Julienne, Chem. Rev. **112**, 4949 (2012).
[3] K.-K. Ni, S. Ospelkaus, M. H. G. de Miranda, A. Pe'er, B. Neyenhuis, J. J. Zirbel, S. Kotochigova, P. S. Julienne, D. S. Jin, and J. Ye, Science **322**, 231 (2008).
[4] S. Ospelkaus, K.-K. Ni, D. Wang, M. H. G. de Miranda, B. Neyenhuis, G. Quéméner, P. S. Julienne, J. L. Bohn, D. S. Jin, and J. Ye, Science **327**, 853 (2010).
[5] T. Takekoshi, L. Reichsöllner, A. Schindewolf, J. M. Hutson, C. R. Le Sueur, O. Dulieu, F. Ferlaino, R. Grimm, and H.-C. Nägerl, Phys. Rev. Lett. **113**, 205301 (2014).
[6] P. K. Molony, P. D. Gregory, Z. Ji, B. Lu, M. P. Köppinger, C. R. Le Sueur, C. L. Blackley, J. M. Hutson, and S. L. Cornish, Phys. Rev. Lett. **113**, 255301 (2014).
[7] J. W. Park, S. A. Will, and M. W. Zwierlein, Phys. Rev. Lett. **114**, 205302 (2015).
[8] M. Guo, B. Zhu, B. Lu, X. Ye, F. Wang, R. Vexiau, N. Bouloufa-Maafa, G. Quéméner, O. Dulieu, and D. Wang, Phys. Rev. Lett. **116**, 205303 (2016).
[9] T. M. Rvachov, H. Son, A. T. Sommer, S. Ebadi, J. J. Park, M. W. Zwierlein, W. Ketterle, and A. O. Jamison, Phys. Rev. Lett. **119**, 143001 (2017).
[10] X. Ye, M. Guo, M. L. González-Martínez, G. Quéméner, and D. Wang, Sci. Adv. **4**, eaaq0083 (2018).
[11] M. Mayle, B. P. Ruzic, and J. L. Bohn, Phys. Rev. A **85**, 062712 (2012).
[12] M. Mayle, G. Quéméner, B. P. Ruzic, and J. L. Bohn, Phys. Rev. A **87**, 012709 (2013).
[13] A. Christianen, M. W. Zwierlein, G. C. Groenenboom, and T. Karman, arXiv:1905.06846.
[14] G. Quéméner and J. L. Bohn, Phys. Rev. A **81**, 022702 (2010).
[15] G. Wang and G. Quéméner, New J. Phys. **17**, 035015 (2015).
[16] L. Lassablière and G. Quéméner, Phys. Rev. Lett. **121**, 163402 (2018).
[17] T. Karman and J. M. Hutson, Phys. Rev. Lett. **121**, 163401 (2018).
[18] A. Micheli, Z. Idziaszek, G. Pupillo, M. A. Baranov, P. Zoller, and P. S. Julienne, Phys. Rev. Lett. **105**, 073202 (2010).
[19] M. H. G. de Miranda, A. Chotia, B. Neyenhuis, D. Wang, G. Quéméner, S. Ospelkaus, J. L. Bohn, J. Ye, and D. S. Jin, Nat. Phys. **7**, 502 (2011).
[20] A. Chotia, B. Neyenhuis, S. A. Moses, B. Yan, J. P. Covey, M. Foss-Feig, A. M. Rey, D. S. Jin, and J. Ye, Phys. Rev. Lett. **108**, 080405 (2012).
[21] A. Simoni, S. Srinivasan, J.-M. Launay, K. Jachymski, Z. Idziaszek, and P. S. Julienne, New J. Phys. **17**, 013020 (2015).
[22] A. van der Avoird, P. E. S. Wormer, and R. Moszynski, Chem. Rev. **94**, 1931 (1994).
[23] M. Lepers, R. Vexiau, M. Aymar, N. Bouloufa-Maafa, and O. Dulieu, Phys. Rev. A **88**, 032709 (2013).
[24] G. E. Karniadakis and S. J. Sherwin, *Spectral/hp Element Methods for Computational Fluid Dynamics*, 2nd ed. (Oxford University Press, Oxford, 2005).
[25] A. Simoni, A. Viel, and J.-M. Launay, J. Chem. Phys. **146**, 244106 (2017).
[26] Z. Idziaszek and P. S. Julienne, Phys. Rev. Lett. **104**, 113202 (2010).
[27] A. V. D. Avoird, P. E. S. Wormer, F. Mulder, and R. M. Berns, Top. Curr. Chem. **93**, 1 (1980).
[28] R. V. Krems and A. Dalgarno, J. Chem. Phys. **120**, 2296 (2004).
[29] A. Micheli, G. Pupillo, H. P. Büchler, and P. Zoller, Phys. Rev. A **76**, 043604 (2007).
[30] J. L. Bohn, M. Cavagnero, and C. Ticknor, New J. Phys. **11**, 055039 (2009).
[31] S. Kotochigova, New J. Phys. **12**, 073041 (2010).
[32] B. Friedrich and D. Herschbach, J. Phys. Chem. A **103**, 10280 (1999).
[33] A. V. Avdeenkov, M. Kajita, and J. L. Bohn, Phys. Rev. A **73**, 022707 (2006).
[34] G. Quéméner and J. L. Bohn, Phys. Rev. A **83**, 012705 (2011).
[35] P. S. Julienne, T. M. Hanna, and Z. Idziaszek, Phys. Chem. Chem. Phys. **13**, 19114 (2011).

[36] T. V. Tscherbul and A. Dalgarno, J. Chem. Phys. **133**, 184104 (2010).
[37] Y. V. Suleimanov, T. V. Tscherbul, and R. V. Krems, J. Chem. Phys. **137**, 024103 (2012).
[38] G. F. Gribakin and V. V. Flambaum, Phys. Rev. A **48**, 546 (1993).
[39] A. Simoni and J.-M. Launay, J. Phys. B **44**, 235201 (2011).
[40] A. Dawid, M. Lewenstein, and M. Tomza, Phys. Rev. A **97**, 063618 (2018).
[41] H. Terrier, J.-M. Launay, and A. Simoni, Phys. Rev. A **93**, 032703 (2016).